Journal of
Mechanics of
Materials and Structures

A COHESIVE ZONE FINITE ELEMENT APPROACH TO MODEL TENSILE CRACKS IN THIN FILM COATINGS

Srikant Nekkanty, Mark E. Walter and Rajiv Shivpuri

Volume 2, Nº 7 September 2007

mathematical sciences publishers

JOURNAL OF MECHANICS OF MATERIALS AND STRUCTURES
Vol. 2, No. 7, 2007

A COHESIVE ZONE FINITE ELEMENT APPROACH TO MODEL TENSILE CRACKS IN THIN FILM COATINGS

SRIKANT NEKKANTY, MARK E. WALTER AND RAJIV SHIVPURI

A two-dimensional finite element model using cohesive zone elements was developed to predict cracking in thin film coating-interlayer-substrate systems that are subjected to tensile loading. The constitutive models were chosen to represent a metal carbide/diamond-like carbon composite coating with a titanium interlayer and a steel substrate. Material properties of the coating and interlayer along with the cohesive finite element parameters were varied to study effects on stress distributions and coating cracking. Stress distributions were highly nonuniform through the coating thickness. Thus the initiation and arrest of tensile cracks differed from what is predicted by simple shear-lay theory. Intercrack spacing distributions resulting from the variation of different parameters were quantified and compared with those from experiments.

1. Introduction

Coating systems provide enabling technologies that have enhanced productivity for a wide variety of applications. Hard coatings are a class of coating that has been developed as a surface engineering enhancement solution for cutting tools, dies, drills, and other tribological applications. All of these applications rely on the fact that the coatings are extremely hard, abrasion-resistant, and/or provide low-friction surfaces. Most hard coatings are ceramic compounds such as carbides, nitrides, ceramic alloys, cermets, and metastable materials such as diamond and cubic boron nitride. Their properties and environmental resistance depend on composition, stoichiometry, impurities, microstructure, and texture. To effectively design coating systems for specific applications, it is necessary to know the chemical, mechanical, and tribological properties of the coatings.

To a large extent, adhesion at the coating-substrate interface and toughness of the coating itself determines the durability of hard coating systems. Loss of adhesion at the coating-substrate interface leads to premature failure of otherwise wear resistant and tough coatings. There have been many investigations of failure properties of coatings using indentation [Begley and Hutchinson 1998; Rabiei et al. 1999]. Investigations have measured the adhesion of brittle films on a ductile substrate [Li and Bhushan 1998] and have observed preferred pathways for local cracking and separation in thermal spray coatings [Nekkanty and Walter 2004]. Li and Bhushan [1998] have used indentation techniques to measure the fracture toughness of thin, amorphous carbon films. Previous work by the authors presented the results of Vickers indentation experiments carried out on four different boron carbide/diamond-like carbon (DLC) composition coatings that were sputter deposited onto 52100 steel disks [Nekkanty and Walter 2004]. Although the indentation depths for these experiments ranged from less than 10% of the coating thickness to many times more than the coating thickness, qualitative comparisons of coating toughness were made.

Keywords: thin film coatings, cohesive zone finite element modeling, tensile cracking, intercrack spacing.

There have been numerous investigations to explore indentation coating failure using numerical methods. Begley et al. [2000] analyzed a wedge impression test for measuring interface toughness between films and substrates using numerical methods. Chen et al. [2005] recently developed numerical methods to explore the mechanics of indentation-induced lateral cracking. Based on finite element analysis (FEA) of spherical indentation of a thin hard film deposited on a soft substrate, Sriram et al. [2003] have carried out studies to understand the mechanics of film fracture. Theoretical issues surrounding the extraction of elastic and plastic properties from indentation load versus displacement data have also advanced; however, there are still a number of ambiguities surrounding actual physical processes involving indentation of such small volumes (for example, [Brotzen 1994; VanLandingham 2003]). Equipment calibration also becomes critical at such small displacements and loads.

Scratch testing is a widely used technique for evaluating the adhesion of thin, hard coatings. Scratch testing is useful to compare the adherence of similar coating-substrate systems; however, it fails to *quantify* parameters such as interfacial strength between the coating and the substrate and cohesive strength of the coating. A novel method for evaluating adhesion strength was proposed by Agrawal and Raj [1989]. This tensile cracking approach evaluates both the cohesive strength of the coating and the interfacial adhesion strength between the coating and the substrate. The approach is based on subjecting a brittle coating on a ductile substrate to tension and thereby propagating coating cracks that are oriented transverse to the tensile direction. A micrograph showing transverse cracks in a tungsten carbide/DLC (WC-DLC) coating on a stainless steel tensile specimen is shown in Figure 1. The crack density increases with substrate tension until the crack spacing reaches a saturation value when it is no longer influenced by the increase in substrate tension. The model relates $\hat{\tau}$, the interfacial shear strength between the coating and the substrate to $\hat{\sigma}$, the tensile fracture strength of the film, $\hat{\lambda}$, the characteristic saturation crack spacing, and δ, the coating thickness [Agrawal and Raj 1989] as

$$\hat{\tau} = \frac{\pi \delta \hat{\sigma}}{\hat{\lambda}}. \tag{1}$$

For a highly elastic coating, the tensile strength of the coating, $\hat{\sigma}$ can be written as

$$\hat{\sigma} = E\varepsilon_f, \tag{2}$$

where E is the modulus of elasticity of the coating and ε_f is the strain corresponding to the onset of cracking in the coating.

Agrawal and Raj [1989] proposed the full sine wave function shown in Figure 2a for approximating the interfacial shear stress. This approximation results in zero interfacial shear stress values at the mid point and at both ends of the intercrack spacing in the coating. Other research groups have asserted that, as shown in Figure 2b, the interfacial shear stress should have its maximum value located at each end of the intercrack spacing and be zero at the midpoint of the intercrack spacing in the coating [Wojciechowski and Mendolia 1989; Yanaka et al. 1998; Chen et al. 1999; 2000]. The recent analytical work of Yanaka et al. [1998] and Wojciechowski and Mendolia [1989], and the experiments and FEA of Chen et al. [1999; 2000], indicate that the interfacial shear stress distribution is best approximated by a distribution like the one shown in Figure 2b. The applicability of these two different shear stress distributions may be related to how the crack spacing compares to the coating thickness.

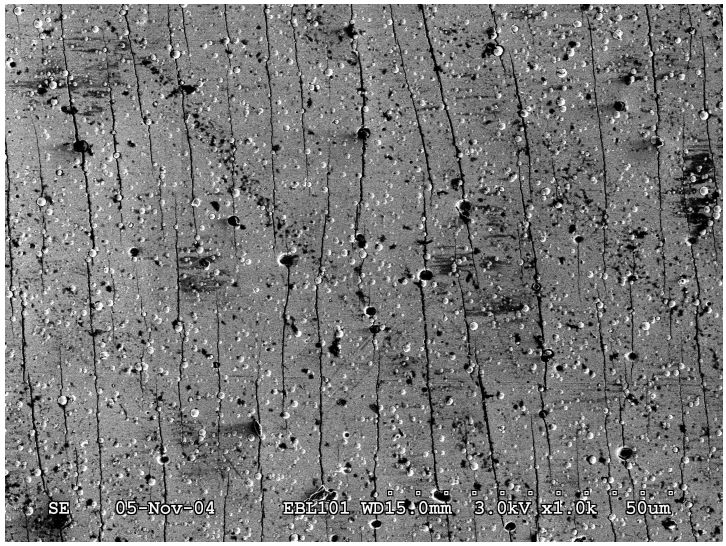

Figure 1. WC-DLC coating pulled to 4% strain resulting in longitudinal cracks. Tensile direction is perpendicular (horizontal in the figure) to the longitudinal cracks.

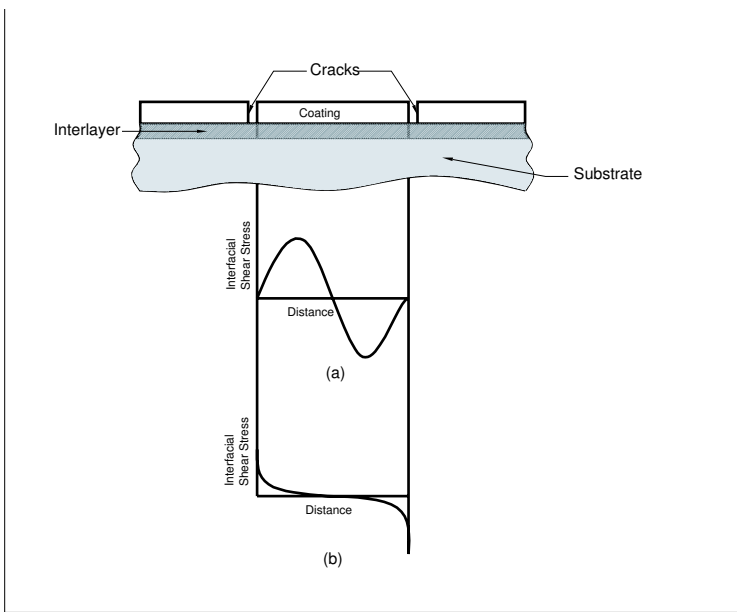

Figure 2. Two different theories predicting the distribution of interfacial shear stresses along the coating-interlayer interface between two cracks when the coating-interlayer-substrate system is subject to tensile loads: (a) sinusoidal distribution with zero stress at the endpoints [Agrawal and Raj 1989], and (b) maximum stress at the endpoints [Chen et al. 2000; Yanaka et al. 1998; Wojciechowski and Mendolia 1989].

The previous work with finite element analysis of tensile cracking assumes preexisting cracks by introducing fine notches in the model [Wojciechowski and Mendolia 1989; Yanaka et al. 1998; Chen et al. 1999; 2000; Krishnamurthy and Reimanis 2005]. Few researchers have developed finite element models which can simulate the formation and propagation of tensile cracks and thus predict coating performance. The present work uses cohesive zone elements to model crack development in the coating. After calibration with simple tensile cracking experiments, the finite element model could be used to predict the behavior of the coating-substrate system for the more complex loadings associated with actual applications. The next section of this paper describes the finite element model and the various physical and numerical parameters. The model is based on tensile cracking experiments that were carried out with WC-DLC coatings on 310 stainless steel substrates. The third section presents results for varying model parameters, and the final section then discusses the resulting simulated tensile cracking behavior.

2. Finite element model description

An idealization of the coating system that was modeled is shown in Figure 3a. Figure 3b shows the magnified view of the coating showing where cohesive elements were placed. The ABAQUS 6.5.1 commercial FEA package was used for all the modeling. As indicated above, the model was loosely based on tensile cracking experiments with WC-DLC coatings. The coating was 1.3 μm thick and was assumed to be homogeneous, isotropic, and perfectly elastic. The 310 stainless steel substrate followed an elastic-plastic material model with linear strain hardening.

The substrate thickness was 230 times the coating thickness. A 1.3 μm thick elastic-plastic titanium interlayer was present between the coating and substrate. Base values for the substrate properties were obtained from in-house experiments. Base values for the coating modulus and interlayer properties, henceforth referred to as the reference case, were obtained from [Voevodin et al. 1999] and www.matweb.com, respectively. The coating is assumed to be homogeneous along the thickness. The material properties for the substrate, coating, and interlayer are provided in Table 1. Four-node (QUAD4) plane strain elements were used for the analysis. As shown in Figure 3, symmetry boundary conditions were applied along the bottom of the model, and displacements were applied at the right and left edges. Displacements were specified at the edge nodes of the substrate and interlayer but not on the coating. The maximum displacement values were such that the strain in the direction of the loading was 4%. The final 4% strain value was chosen to be consistent with experiments.

Cohesive zone finite elements were placed through the thickness of the coating. These bilinear elements are available in the standard ABAQUS element library. The cohesive behavior assumes a linear elastic traction separation law prior to damage and a linear damage evolution based on energy dissipated due to failure, G_C. The input parameters for the cohesive elements are further described below. The layout of these elements is shown in Figure 3b. In the middle of the coating the distance between each row of cohesive zone elements is 1 μm. Away from the middle of the model, the spacing was increased to 10 μm. In this way, computational expense was reduced while focusing on a region that is far away from any edge effects. The interface is assumed to be perfectly bonded, and therefore there are no cohesive elements along the interface. This assumption is based on industry experience with state of the art PVD thin film coatings. In addition, Wang et al. [1998] have predicted that the interface toughness is greater than 150 J/m^2, while the film toughness is approximately 30 J/m^2 for DLC films on steel substrates.

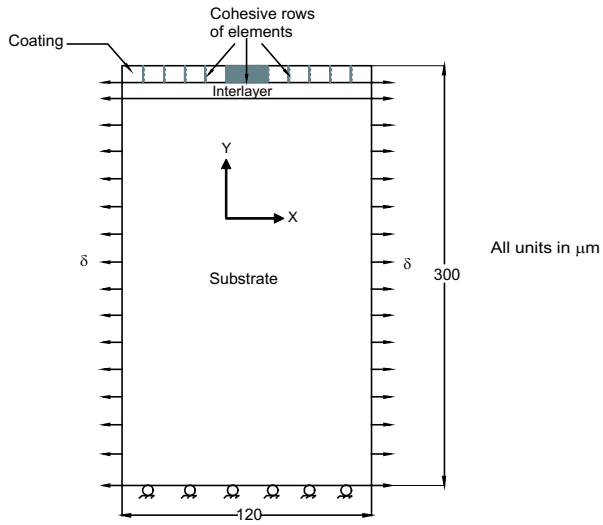

(a)

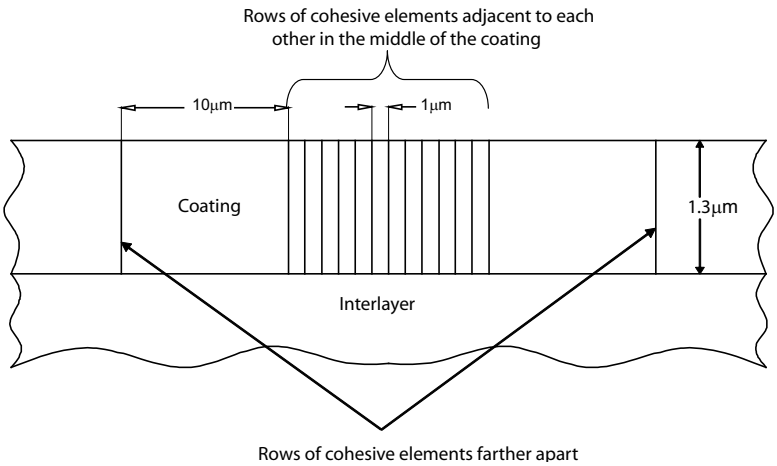

(b)

Figure 3. (a) Schematic of the FE model (not to scale); (b) illustration of cohesive zones in the coating (magnified view of (a)).

As shown in Figure 4, the response of the cohesive zone element is determined by specifying K, the loading slope or cohesive stiffness, σ_C, the critical normal stress, and G_C, the area under the traction versus displacement curve. The area under the traction versus displacement curve is called G_C because it is a measure of the critical energy release rate. Values for the cohesive zone element parameters are provided in Table 1. The critical normal stress values were estimated based on experiments with acoustic emission [Nekkanty and Walter 2006]. From experiments, the strain corresponding to the onset of cracking was estimated to be 1.2%. The critical normal stress, σ_C, can then be obtained from Equation (2). Similar strain values were also observed by Wang et al. [1998]. The baseline G_C values used in

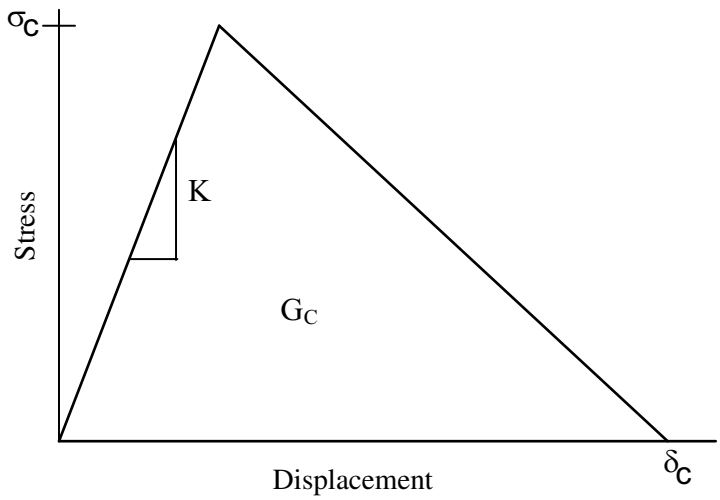

Figure 4. Bilinear law followed by the cohesive elements used in the study. Cohesive elements have a stiffness K and fail when the critical stresses in the elements reach beyond the critical stress σ_C.

this study were consistent with those predicted by Wang et al. [1998]. The cohesive stiffness was held constant for all cohesive zone elements.

Although at a given location in the coating the cohesive parameters were kept the same for all the coating through-thickness lines of cohesive zone elements, the σ_C and G_C parameters were allowed to vary along the x-direction. The different σ_C values were obtained by using MATLAB's random number generator to generate uniformly distributed values in a prescribed range. The range of variation for σ_C was ± 75 MPa. The critical separation (δ_C, in Figure 4) was held constant, and therefore the range of variation for G_C was 32-37 J/m^2. The random assignment of different parameter values to different cohesive zone elements served the following two purposes: (a) it simulated the natural, statistical variation of the coating's cohesive strength, and (b) the different values of critical stresses in different cohesive zones ensured that not all the cohesive zone elements failed together when the critical tensile load was reached.

The modeling of progressive damage involves softening of the material response, which leads to convergence difficulties in an implicit solution procedure. To overcome such convergence problems, ABAQUS/Standard implements a viscous regularization parameter. This parameter regularizes the traction separation laws by permitting stresses to be just outside the limits set by the traction separation law. Using a small value for the viscosity regularization parameter improves the rate of convergence of the model in the softening regime and does not alter the sequence of cracking. Detailed discussion of this parameter can be found in [ABAQUS 2005; Alfano and Crisfield 2001]. The parameter was kept the same for all the cohesive zone elements. By trial and error, the smallest value that still produced converged solutions was used. The solution was carried out using implicit analysis and converged in approximately 550 total iterations. Up to the point where cohesive elements would start failing, the stresses in the coating were found to be the same in the models without and with cohesive elements.

This indicates that the inclusion of the cohesive elements was not altering the stress state before damage initiation.

The model was also checked for mesh convergence. The original mesh scheme described above (5 elements between two neighboring cohesive elements in the middle of the coating, and 9 elements along the thickness of the coating) was compared with two other mesh schemes: a coarser mesh containing 3 elements between two neighboring cohesive elements in the middle of the coating and 5 elements along the thickness of the coating, and a refined mesh containing 8 elements between two neighboring cohesive elements in the middle of the coating and 13 elements along the thickness of the coating. Figure 5 shows the horizontal-direction normal stress along the surface of the coating, and plotted for a region with higher cohesive element density. The three different mesh schemes are shown at 2% strain. From Figure 5, since there is little difference between the original and refined meshes, it is assumed that mesh convergence was achieved with the original mesh.

3. Results

In order to explore the effect of various parameters on the model response, one set of parameters was designated as the reference case (see Table 1). The subsequent studies were variations on the reference case. The next two subsections discuss the stress distributions in the reference case and the effect of variation of different parameters with respect to the reference case.

		Reference case	Mod. #1	Mod. #2	Mod. #3	Mod. #4
Coating	Modulus (GPa)	200	300	200	200	200
	Poisson ratio	0.3	0.3	0.3	0.3	0.3
Substrate properties	Modulus (GPa)	200	200	200	200	200
	Poisson ratio	0.2	0.2	0.2	0.2	0.2
	Yield strength (MPa)	200	200	200	200	200
	Tangent modulus of plastic region	2000	2000	2000	2000	2000
Interlayer properties	Modulus (GPa)	110	110	110	110	110
	Poisson Ratio	0.3	0.3	0.3	0.3	0.3
	Yield strength (MPa)	140	140	140	140	140
	Strain hardening slope (MPa)	720	720	1440	360	720
Cohesive properties	Critical stress (σ_C)	2500–2650	2500–2650	2500–2650	2500–2650	1500-1650
	G_C (J/m^2)	32–37	32–37	32–37	32–37	32–37

Table 1. Coating, interlayer, and substrate properties used for the different simulations.

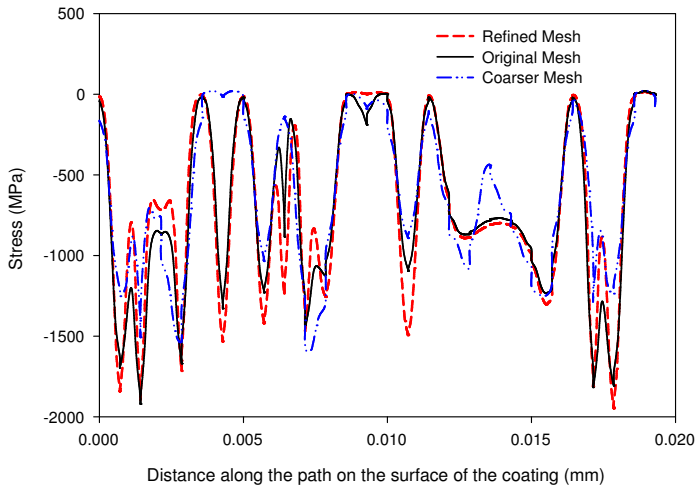

Figure 5. Horizontal-direction normal stress profiles at 2% strain along the surface of the coating for 3 different mesh schemes.

3.1. ***Stress distributions.*** For the reference case, when the normal stress in the tensile direction (σ_{xx}) in the coating exceeds the smallest random σ_C value, the first crack(s) appear. The tractions on the newly formed crack faces go to zero, and therefore the coating stresses are redistributed. An example of two σ_{xx} surface stress contours between two cracks which are 20 μm apart is shown in Figure 6. Since the σ_{xx} surface stress is zero at the cracks, both edges of the plot show zero stress. For the ith load increment,

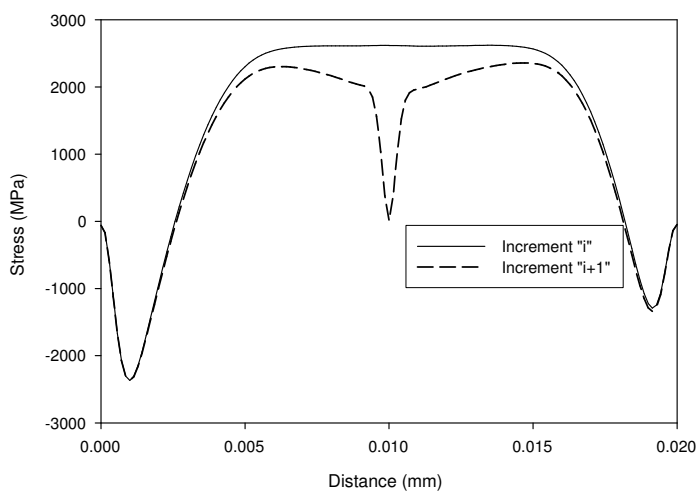

Figure 6. Evolution of tensile stresses between two cracks 20 microns apart with the increase in load.

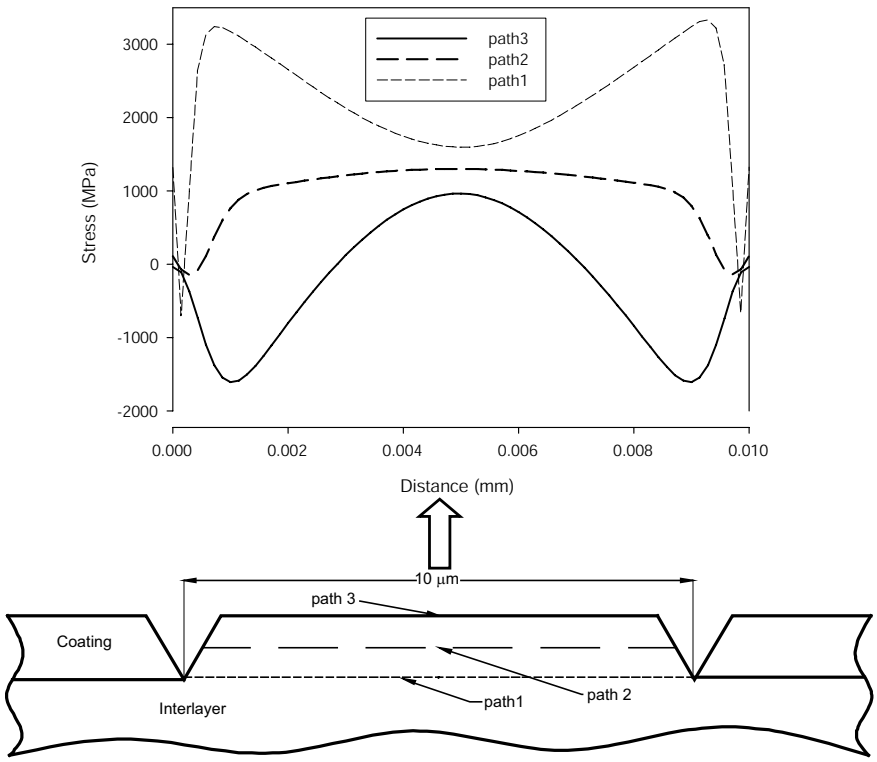

Figure 7. Normal stress distribution along paths in the coating between two cracks 10 microns apart.

the stress is still uniform in the middle region between the two cracks. In the $i + 1$' increment the stress in the middle of the region of interest has exceeded the critical value for one of the cohesive zone elements, a new crack is generated, and the σ_{xx} surface stresses go towards zero. This crack progression is consistent with the shear lag models for tensile cracking [Agrawal and Raj 1989; Wojciechowski and Mendolia 1989; Yanaka et al. 1998; Chen et al. 1999; 2000].

From shear lag assumptions and from the above description of the contours in Figure 6, one would expect the cracks always to form at the midpoint between two adjacent cracks. However, this expectation is based on the assumption that the stress profile in Figure 6 is unchanged through the thickness of the coating. Uniform stresses along the thickness of the coating are also an underlying assumption in the analytical models referred to above [Agrawal and Raj 1989; Wojciechowski and Mendolia 1989; Yanaka et al. 1998; Chen et al. 1999; 2000]. It was found that the stresses are not uniform through the coating thickness. Since one side of the coating is free and the other side is bound to the interlayer, stresses should vary through the thickness of the coating. The crack formed at the midpoint in Figure 6 because of the particular combination of geometric and materials parameters.

In Figure 7, for the region between two cracks that are 10 μm apart (there are no cohesive elements between these cracks) the σ_{xx} stress profiles are plotted for paths at different coating depths. The stress

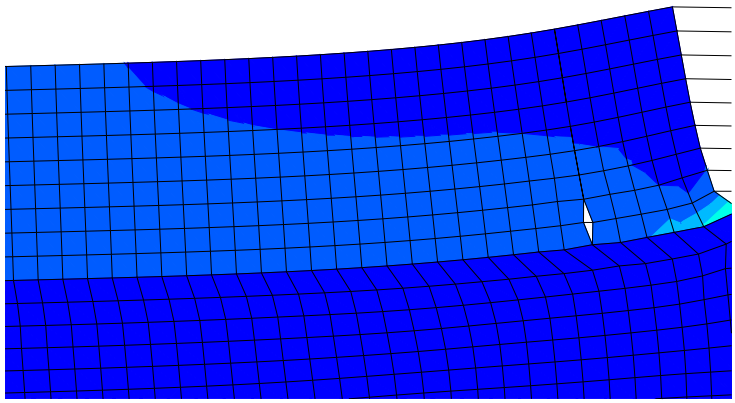

Figure 8. Crack in the coating originating from the interface.

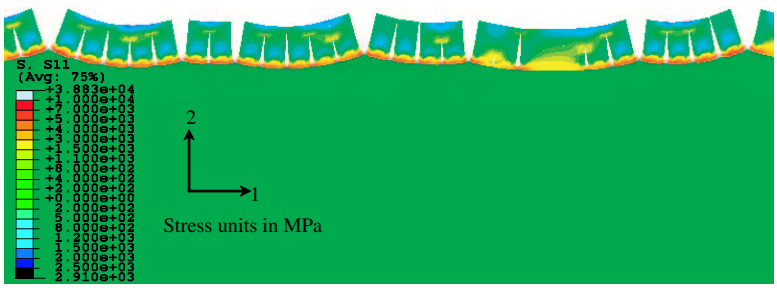

(a)

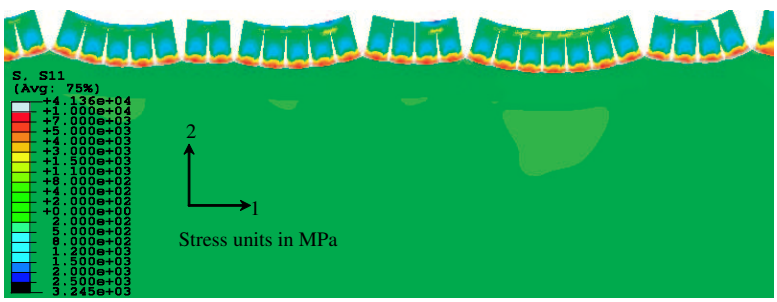

(b)

Figure 9. Cracks in the coating for reference model: (a) 2.5% strain, and (b) 4% strain. Notice the crack arrest.

profiles are not at all self-similar, and the location of the maximum σ_{xx} is not always at the midpoint between two adjacent cracks. In particular, the highest σ_{xx} stresses are found close to the interface and close to the existing cracks. Figure 7 also serves to highlight that near-crack stresses along the surface of the coating are compressive, and near-crack stresses near the interface are tensile. All stresses become tensile as one approaches the midpoint of the region. A similar stress distribution was observed by Krishnamurthy and Reimanis [2005].

As shown in Figure 8, the internal stresses and boundary conditions on an unbroken coating segment are such that the coating undergoes significant bending. The bending of the coating results in compressive near-crack stresses close to the surface of the coating. This stress distribution has important implications for crack propagation, with the high tensile near-crack stresses close to the interface suggesting that the cracks will originate from the interface. Indeed, the tensile cracking experiments performed by Krishnamurthy and Reimanis [2005] indicated that cracks may be originating from the interface.

The near-crack compressive stresses that exist closer to the surface of the coating will cause cracks originating from the interface to be arrested. Figure 9 shows a longer portion of the cracked coating for 2.5% and 4% overall strain, respectively. Figure 9 shows that, although multiple cracks originating from the interface were present at 2.5% strain, there was little or no continued crack propagation towards the surface even after 4% strain. If the coating is examined from the top and in the direction of the loading, the number of cracks reaching the surface becomes constant at higher strain levels. In other words the inter-crack spacing has saturated.

3.2. ***Parameter study.*** As shown in Table 1, the first modification of the reference case was increasing the modulus of the coating. All other material and cohesive parameters were kept the same. The higher coating modulus resulted in higher stresses at lower overall strains and, as expected, the fracture strain (the strain at which the first crack appears) decreased. Furthermore, as a result of the higher stresses in the coating, it can be seen from Figure 10a that more cracks have progressed from the interface to the surface of the coating.

The second modification to the reference case model was made by increasing the slope of the tangent modulus for the plastic region of the interlayer. This essentially increased the strain hardening of the interlayer. It can be seen in Figure 10b that compared to the reference case, more cracks have progressed from the interface to the surface of the coating. This results from the higher stresses in the interlayer for the same amount of strain as compared to the reference case. With a less deformable interlayer, the unbroken coating segment does not bend as much and therefore the near-crack compressive stresses close to the surface of the coating are diminished. As a result, cracks can more readily propagate to the surface.

A third modification to the reference model was made by decreasing the slope of the tangent modulus for the plastic region of the interlayer. This change has the overall effect of making the interlayer more deformable. The contour plot in Figure 10c shows that there is more curvature of the segments and the cracks have larger openings. The curvature of the coating increases due to the increase in the softening of the interlayer. The increase in the curvature results in an increase of the compressive stresses near the surface of the coating. Consequently, there are fewer cracks progressing to the surface. Also, there is an increase in the curvature of the interface as well. This leads to the higher tensile stresses near the interface, and as a result, more cracks originate from the interface compared to the reference case. This can be seen in Figure 11 where σ_{xx} stress profiles between two cracks are plotted at the surface of the coating and near the interface (paths 3 and 1 of Figure 7) for the two different interlayer cases.

For the last modification of the reference case, the σ_C values of all the cohesive zone elements were decreased by 1000 MPa compared to the reference case while keeping G_C the same. Decreasing σ_C while keeping G_C constant essentially decreases the softening slope of the cohesive zone element and, hence, the critical separation (δ_C, in Figure 4) increases. These changes result in a decrease in the fracture strain compared to the reference case. When compared with the reference case, at 2% strain, Figures 12a

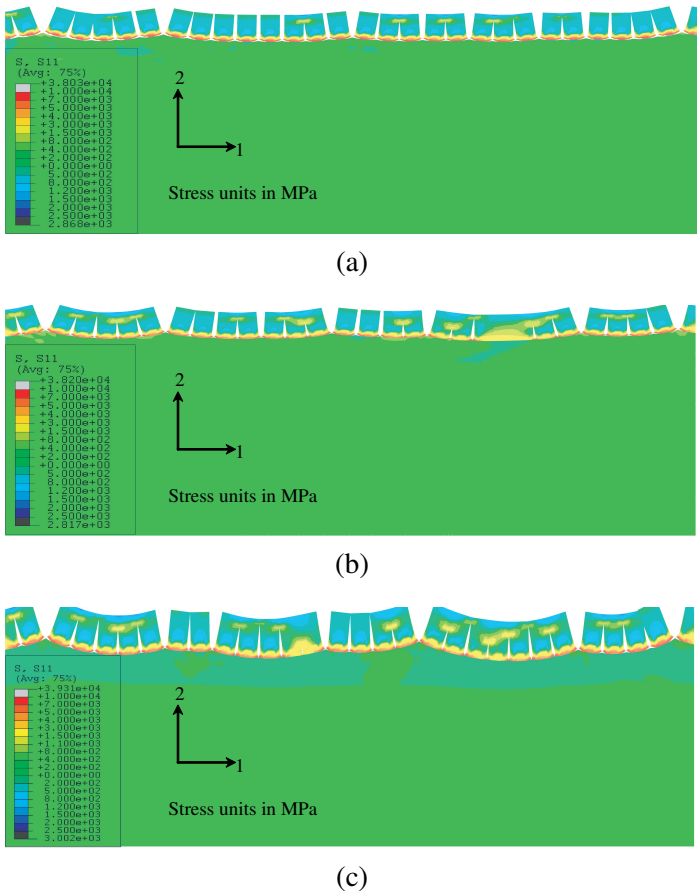

Figure 10. Change in cracks from reference model due to: (a) increase in coating modulus; (b) increase in tangent modulus slope in interlayer; and (c) decrease in tangent modulus slope in interlayer. All images correspond to 2.5% strain.

and 12b show that the decreased σ_C results in more cracks being generated. It could be argued that if the reference case coating-substrate system were pulled to higher strains, then more cracks would propagate to the surface. However, as will be discussed in the next section, there are assumptions with the two-dimensional model that need to be taken into account before making such an argument.

4. Discussion

The above parameter study indicates that cracking in the coating is sensitive to the material properties of the coating and interlayer and also to the cohesive zone element parameters. The model also demonstrates surface level crack saturation which means that no new cracks will appear on the surface with increasing tensile strain. Shear lag analysis of tensile cracking that includes the assumption of uniform through-thickness stresses predicts that the crack spacing will saturate [Agrawal and Raj 1989; Wojciechowski and Mendolia 1989; Yanaka et al. 1998; Chen et al. 1999; 2000]. The current simulations indicate that

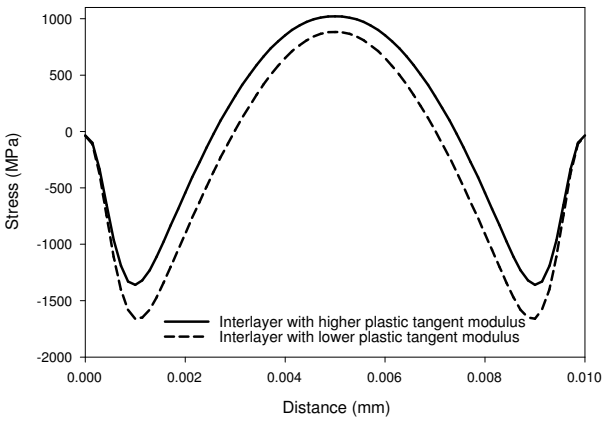

(a)

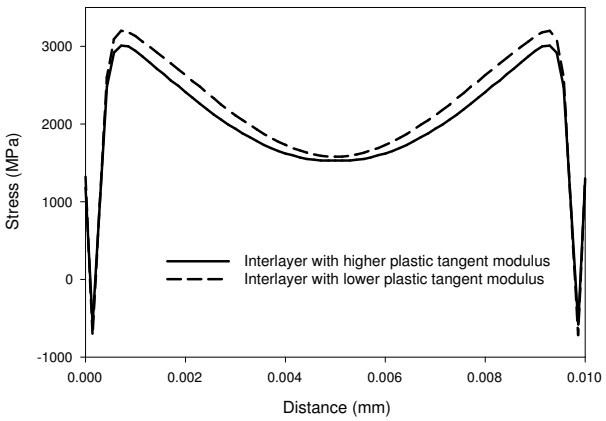

(b)

Figure 11. Comparison of σ_{xx} stresses between two cracks 10 μm apart for two interlayer cases: (a) stresses at the surface of the coating, and (b) stresses near the coating-interlayer interface.

(a)

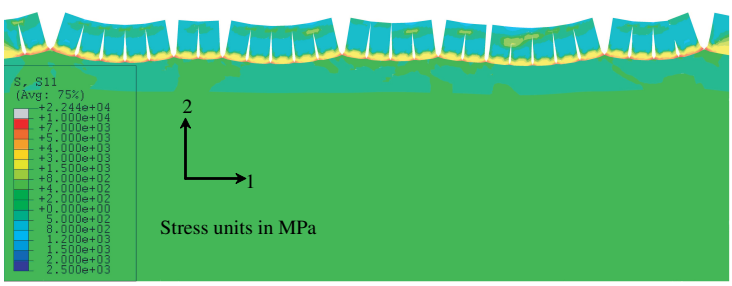

(b)

Figure 12. Differences in the formation of cracks for 2% strain: (a) reference case, and (b) decreased σ_C.

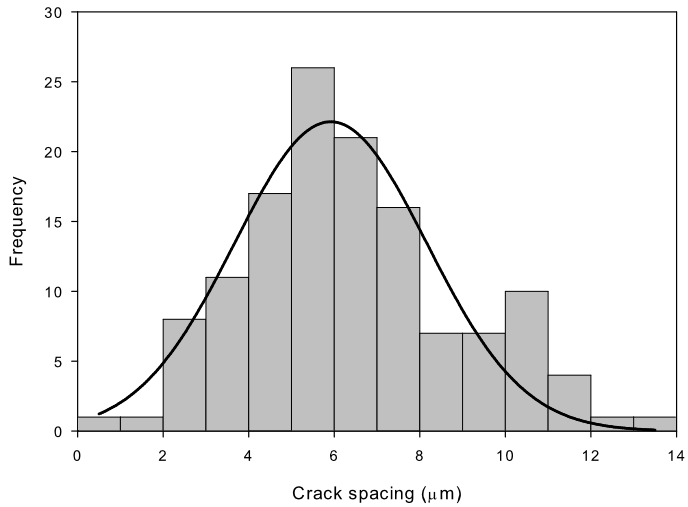

Figure 13. Distribution of intercrack spacing for WC/DLC coating pulled to 4% strain.

although the crack saturation can exist at the coating surface level, there may be subsurface cracks that have not propagated all the way to the surface.

In the current model, further straining of the coating substrate system would eventually cause all cracks to propagate to the surface. However, this situation is the result of having a two-dimensional model. In reality, the stress state is no longer uniaxial at very high strains. The triaxial nature of the stress state in the plastic region causes slant cracks at approximately 45° to the existing transverse cracks appear in the coating [Chen et al. 1999]. The existence of these slant cracks is a fair indication that strains are beyond the surface saturation strains and that the stress state is no longer uniaxial. Without a three-dimensional model, slant cracks cannot be modeled. Experimental results for the WC-DLC system indicated that slant crack began at approximately 4.5% strain. For this reason, the current simulations were run to 4% strain.

The distribution of the crack spacing for the cracks in Figure 1 is given in Figure 13. The mean value of the crack spacing is 6.0 μm with a standard deviation of 2.4. A normal distribution with the given mean and standard deviation values is provided in the same plot. The distributions of crack spacing from the numerical simulations described in Section 3.2 are shown in Figures 14a–d. Only cracks which have propagated all the way to the surface of the coating are included in the distribution plots. As seen from Figure 14a, the mean crack spacing for the reference case is less than that from the experiments. Also, as seen in Figures 14b and 14d, with the increase in coating modulus and the decrease in σ_C, respectively, the distribution of crack spacing is unrealistically small since almost every cohesive element has failed. As expected, Figure 14c shows that the mean crack spacing for the case of increase in tangent modulus slope of the interlayer is less than that of the reference case. It must be pointed that the distributions in Figure 14 are based on a coating span of only 40 μm as compared to the coating span of 130 μm used for the experimental results shown in Figure 13.

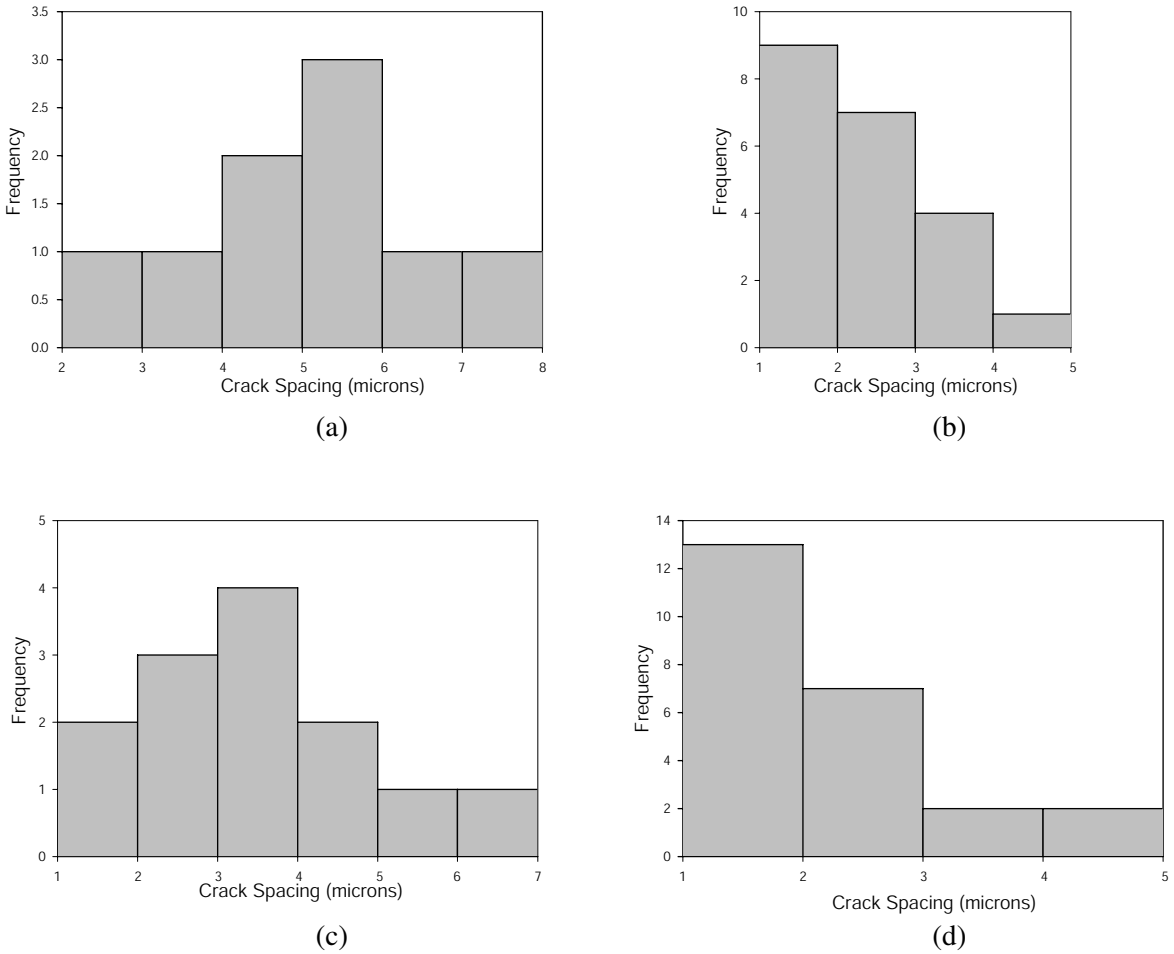

Figure 14. Distribution of intercrack spacing observed in numerical simulation: (a) reference case; (b) increase in coating modulus; (c) increase in tangent modulus slope in interlayer; and (d) decrease in σ_C of cohesive elements.

In the numerical simulations discussed above, the coatings were assumed to be isotropic, homogeneous, and free of defects. However, as seen in Figure 1, pits of various sizes are present on the surface of the coating. Although many of the cracks go through pits, there are also pits without any cracks. More detailed investigation is required to confirm whether or not pits are assisting crack propagation. Microstructural observations would need to be performed in order to determine if there are any additional microstructural inhomogeneities that affect crack spacing.

Investigation of residual stresses was undertaken with compressive residual stresses of 1 GPa as uniform prestresses in the coating. It was observed that inclusion of compressive residual stresses caused the fracture strain (the strain at which the first crack appears) to increase from 1.2% to 1.7%. At lower

strain values, for example, 2%, there are fewer cracks compared to same strain value in the reference case. However at large strain values ($> 4\%$), results look very similar to the reference case results.

5. Summary

A two-dimensional finite element model was created to simulate the response of a coating-interlayer-substrate system to in-plane uniaxial tension. Coating cracking was simulated with cohesive zone elements that followed a bilinear cohesive law. Some degree of randomness was introduced into the model through the assignment of random critical cohesive stresses. Due to the unsymmetrical boundary conditions at the top surface and coating-interlayer interface, bending occurred and introduced nonuniform stresses through the coating thickness. Thus coating cracks propagated from the interface and were often arrested near the surface of the coating by the presence of high compressive stresses. The effects of different coating modulus, tangent modulus for the interlayer hardening, and critical stress values (σ_C) of the cohesive zone elements were studied. The distribution of crack spacing for different parameter changes were quantified and compared to an experimental crack spacing distribution.

Due to the limitations of using a two-dimensional model, crack formation and propagation at high plastic strain values was not predicted accurately. Incorporating measured residual stresses into the model is necessary for more realistic simulations. The model has been shown to be sensitive to material and cohesive parameters and could thus be used to optimize coatings. The described tensile cracking experiment could be used to calibrate cohesive parameters for subsequent modeling of more complicating loading schemes.

References

[ABAQUS 2005] *ABAQUS 6.5 user manual*, Version 6.5, Hibbitt Karlsson Sorensen Inc., Pawtucket, RI, 2005.

[Agrawal and Raj 1989] D. C. Agrawal and R. Raj, "Measurement of the ultimate shear-strength of a metal ceramic interface", *Acta Metall.* **37**:4 (1989), 1265–1270.

[Alfano and Crisfield 2001] G. Alfano and M. A. Crisfield, "Finite element interface models for the delamination analysis of laminated composites: mechanical and computational issues", *Int. J. Numer. Methods Eng.* **50**:7 (2001), 1701–1736.

[Begley and Hutchinson 1998] M. R. Begley and J. W. Hutchinson, "The mechanics of size-dependent indentation", *J. Mech. Phys. Solids* **46**:10 (1998), 2049–2068.

[Begley et al. 2000] M. R. Begley, D. R. Mumm, A. G. Evans, and J. W. Hutchinson, "Analysis of a wedge impression test for measuring the interface toughness between films/coatings and ductile substrates", *Acta Mater.* **48**:12 (2000), 3211–3220.

[Brotzen 1994] F. R. Brotzen, "Mechanical testing of thin-films", *Int. Mater. Rev.* **39**:1 (1994), 24–45.

[Chen et al. 1999] B. F. Chen, J. Hwang, G. P. Yu, and J. H. Huang, "In situ observation of the cracking behavior of TiN coating on 304 stainless steel subjected to tensile strain", *Thin Solid Films* **352**:1-2 (1999), 173–178.

[Chen et al. 2000] B. F. Chen, J. Hwang, I. F. Chen, G. P. Yu, and J. H. Huang, "A tensile-film-cracking model for evaluating interfacial shear strength of elastic film on ductile substrate", *Surf. Coat. Technol.* **126**:2-3 (2000), 91–95.

[Chen et al. 2005] X. Chen, J. W. Hutchinson, and A. G. Evans, "The mechanics of indentation induced lateral cracking", *J. Am. Ceram. Soc.* **88**:5 (2005), 1233–1238.

[Krishnamurthy and Reimanis 2005] S. Krishnamurthy and I. Reimanis, "Multiple cracking in CrN and Cr2N films on brass", *Surf. Coat. Technol.* **192**:2-3 (2005), 291–298.

[Li and Bhushan 1998] X. D. Li and B. Bhushan, "Measurement of fracture toughness of ultra-thin amorphous carbon films", *Thin Solid Films* **315**:1-2 (1998), 214–221.

[Nekkanty and Walter 2004] S. Nekkanty and M. E. Walter, "Indentation damage to boron carbide-DLC coatings with different compositions", *Surf. Coat. Technol.* **183**:1 (2004), 1–9.

[Nekkanty and Walter 2006] S. Nekkanty and M. E. Walter, "Tensile cracking experiments with in situ acoustic emission", 2006.

[Rabiei et al. 1999] A. Rabiei, D. R. Mumm, J. W. Hutchinson, R. Schweinfest, M. Ruhle, and A. G. Evans, "Microstructure, deformation and cracking characteristics of thermal spray ferrous coatings", *Mater. Sci. Eng. A* **269**:1-2 (1999), 152–165.

[Sriram et al. 2003] K. Sriram, R. Narasimhan, and S. K. Biswas, "A numerical fracture analysis of indentation into thin hard films on soft substrates", *Eng. Fract. Mech.* **70**:10 (2003), 1323–1338.

[VanLandingham 2003] M. R. VanLandingham, "Review of instrumented indentation", *J. Res. Natl. Inst. Stand. Technol.* **108**:4 (2003), 249–265.

[Voevodin et al. 1999] A. A. Voevodin, J. P. O'Neill, and J. S. Zabinski, "Tribological performance and tribochemistry of nanocrystalline WC/amorphous diamond-like carbon composites", *Thin Solid Films* **342**:1-2 (1999), 194–200.

[Wang et al. 1998] J. S. Wang, Y. Sugimura, A. G. Evans, and W. K. Tredway, "The mechanical performance of DLC films on steel substrates", *Thin Solid Films* **325**:1-2 (1998), 163–174.

[Wojciechowski and Mendolia 1989] P. H. Wojciechowski and M. S. Mendolia, "On the multiple fracture of low-elongation thin-films deposited on high-elongation substrates", *J. Vac. Sci. Technol. A* **7**:3 (1989), 1282–1288.

[Yanaka et al. 1998] M. Yanaka, Y. Tsukahara, N. Nakaso, and N. Takeda, "Cracking phenomena of brittle films in nanostructure composites analysed by a modified shear lag model with residual strain", *J. Mater. Sci.* **33**:8 (1998), 2111–2119.

Received 24 Jul 2006. Accepted 20 Feb 2007.

SRIKANT NEKKANTY: nekkanty.1@osu.edu
Department of Industrial, Welding and Systems Engineering, Ohio State University, Columbus, OH 43210, United States

MARK E. WALTER: walter.80@osu.edu
Department of Mechanical Engineering, E331 Scott Laboratory, Ohio State University, 201 W. 19th Avenue, Columbus, OH 43210, United States

RAJIV SHIVPURI: shivpuri.1@osu.edu
Department of Industrial, Welding and Systems Engineering, Ohio State University, Columbus, OH 43210, United States